# The effect of frictional forces on energy loss in a circular roller coaster

**Research Question:** *"How does the approach velocity affect the energy dissipation within a circular roller coaster loop?"*

**Nadeem Said**

---

Word count: 3975

## Abstract

This essay sets out to explore the relationship between the approach velocity of a car entering a circular roller coaster and the energy losses incurred as the loop is traversed. The research question addressed is *"how does the approach velocity affect the energy dissipation within a circular roller coaster loop?"*.

In the design of roller coasters, frictional losses are an important factor that have to be accounted for. For the first loop in a series, the frictional losses incurred are a function of the release height. For further loops, it is only the approach velocity that needs to be considered. Much has been written about the effect of frictional losses on the acceleration experienced in circular, and non-circular roller coasters. The effect of the approach velocity on the energy losses incurred is less studied. The primary energy loss is a result of heat dissipation due to frictional forces. This study will assume that heat dissipation due to aerodynamic drag is negligible compared to the dynamic friction between the car and the tracks. The study is limited to the case of circular roller coasters, but can easily be extended to approximate the relationship for clothoid curved coasters.

The theory behind the motion of circular roller coasters is reviewed and a step-wise iteration is constructed to predict the energy losses incurred for varying approach velocities subject to relevant input parameters.

A circular roller coaster is constructed from wood using AutoCAD and a model car is released from varying vertical heights to achieve different approach velocities. The resulting motion of the car is filmed at 240 frames/second (fps) and analyzed using video analysis software. This data is compared to the iterated results. Throughout the experimental design and data collection, care is taken to minimize the presence and effect of uncertainties.

The iteration suggests that both the percentage energy loss and the absolute energy dissipation vary linearly with the input velocity. These predictions are counterintuitive but are supported by the practical data. These findings have important implications in roller coaster design, implying that the percentage energy dissipation is less in high speed rides. This implies that high speed coaster rides are essentially more efficient and as a consequence a larger number of consecutive loops can be achieved.

## Table of Contents

# 1.0 Introduction

## 1.1 Background

The first proto-type roller coasters appeared in Russia in the 18th century. These rides were not roller coasters in the modern sense since they did not contain complete 360 degree loops (Coker). The earliest complete loop roller coasters appeared in the United States at the end of the 19th century (Pescovitz). These coasters were comprised of a single circular loop and extreme changes in "G" force were experienced by the passengers to the extent that spinal injuries were common.

Modern roller coasters avoid sudden changes in "G" force by employing non-circular loops. Clothoid loops with their familiar inverted tear drop shapes are common. Such loops are expensive to construct. Many modern roller coasters are built around an approximation to the clothoid curve. This approximation is comprised of two separate sections, each of which in itself is a circular path, as shown in figure 1 below.

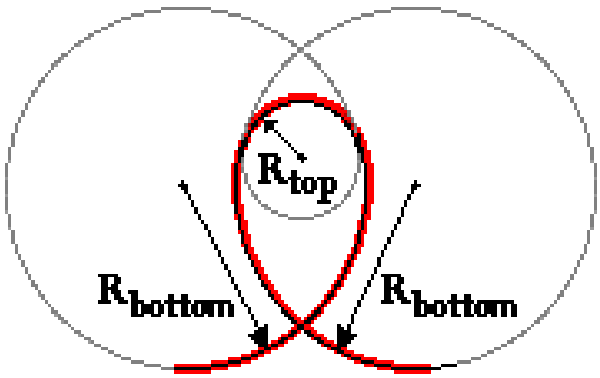


**Fig 1:** The approximation of a clothoid curve, commonly used in many modern roller coasters (The Approximation of a Clothoid).

A key feature in designing a roller coaster ride is energy loss within the loop, and this is the focus of this paper. This paper will study energy losses within a single circular loop, however its findings can be transferred to the bi-circular design in figure

1. The study will be limited to energy losses within a single vertical plane and in this respect will differ from the loops in most amusement parks where lateral twisting is often used to increase the thrill.

Most modern rides consist of a series of loops. In a single loop ride, the engineer can content himself with a knowledge of the absolute heat dissipation within the ride and how it varies with the release height. With multiple loop rides, the engineer is better advised to consider the percentage heat loss within any given loop as a function of the approach velocity and this will be the focus of this paper. The percentage heat loss in consecutive loops is not expected to the same since the approach velocity is reduced. A consequence of this the diminishing radii of consecutive loops shown in figure 2.

**Fig 2:** Multiple loops in the Dragon Khan ride, Spain. Note the reduction in ride radius of consecutive loops (Multiple Loops).

There is little written on the relationship between the energy losses and the approach velocity.

The research question addressed in this paper is: *"how does the approach velocity affect the energy dissipation within a circular roller coaster loop?"*.

The first objective is to study the percentage energy loss variation within a loop with the approach velocity. The second objective is to study the relationship between the absolute energy loss and the approach velocity.

The approach followed in this paper will be to develop a theoretical step-wise iteration to predict the energy losses as a function of angular displacement for various approach velocities. A key input parameter is the coefficient of dynamic friction. A value is attained through use of the iteration and practical measurements of the ride time for given input velocities. The iteration is used to determine the percentage energy loss and absolute loss as a function of the approach velocity. These results are tested against practical measurements.

A roller coaster of radius 0.4m is constructed in the controlled lab environment. The coaster exists in a single plane, so that lateral acceleration is avoided to a large extent but not eliminated entirely due to loop entry requirements. A series of approach velocities are attained through varying the release height. Energy dissipation is determined through measurements of the initial and final velocities through use of video analysis. At all times, care is taken to reduce and account for the presence of experimental uncertainties.

## 1.2.0 Theory

A step-wise iteration of the roller coaster motion in the absence of friction will be developed, and then adjusted to account for the presence of friction. It is necessary to consider the physics behind the motion of the car is it completes a loop.

### 1.2.1 Conservation of angular momentum in a circular roller coaster.

The approach used in this paper, will be to consider the conservation of angular momentum as the car moves through a loop, and then modify the iteration to include friction. Figure 3 shows the external forces acting on the car at points (A, B and C).

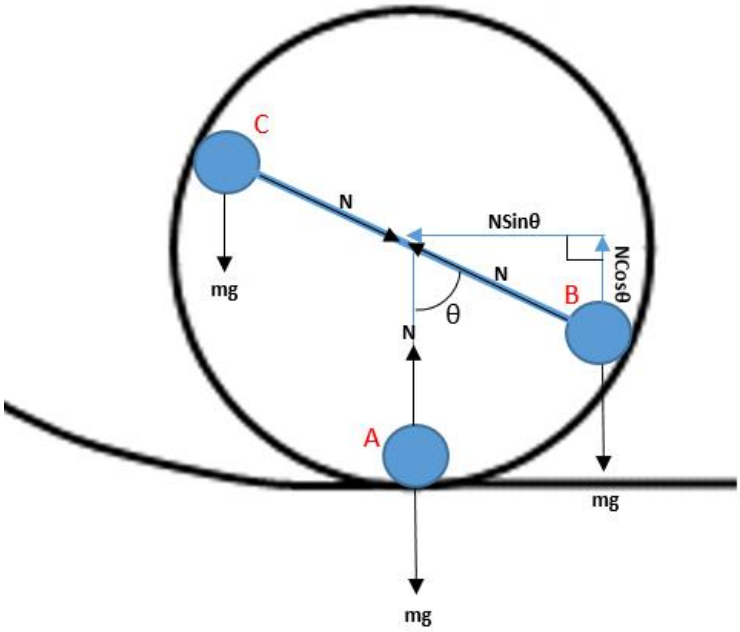


**Fig 3:** The forces acting on a car as it completes a vertical loop

The car enters the loop at point A with a linear velocity $V_0$.

At point A, the angular velocity of the car is given by:

$$\omega_A = \frac{V_0}{r} \quad [1]$$

It follows that the angular momentum as the car enters the loop is given by:

$$\boldsymbol{L} = \boldsymbol{I} \times \frac{\boldsymbol{V_0}}{r} \quad [2]$$

If the car is considered to be a point mass, then the moment of inertia is given by:

$$I = mr^2 \quad [3]$$

Since the car is an extended mass, the approximation gains validity as the loop radius increases. For the radius of 0.4m used in this paper, the approximation in is expected to be valid. The angular momentum of the car is not constant as it moves around the vertical loop since an external torque acts on it. The situation is shown in figure 3.

In the absence of friction, there are two forces acting on the car; the gravitational force and the normal reaction force which is directed towards the center of the circle and whose orientation changes as the car moves around the loop. It is possible to resolve the gravitational force into two perpendicular components as shown in figure 3 such that there exists a component which is parallel to, and acting against, the normal reaction force. This component contributes no torque since it is directed towards the center of the circle. The tangential component is given by:

$$F_{Tangential} = mg \sin\theta \quad [4]$$

Where θ is the angular displacement measured from the vertical. This force provides an external torque on the car given by:

$$\tau = rmg \sin\theta \quad [5]$$

This torque results in an angular acceleration of the car at point B, given by:

$$\dot{\omega} I = -mg \sin\theta \quad [6]$$

The negative sign is included since the torque opposes the angular velocity in the domain $0 < \theta < \pi$.

Inserting [3] into [6] gives:

$$\dot{\omega} = \frac{-g \sin\theta}{r^2} \quad [7]$$

### 1.2.2 A numerical iteration for the relationship between the KE and PE in the absence of friction.

For a numerical analysis of the energy changes as a function of the approach velocity in the absence of friction, two input parameters are required, that of the approach velocity and the radius of the loop. Microsoft Excel is used to perform a step-wise iteration. A screen shot of the initial three steps in the iteration is shown below.

| | A | B | C | D | E | F | G | H |
|---|---|---|---|---|---|---|---|---|
| 1 | | $H_o$/ m | 1.5 | | | | | |
| 2 | | $V_o$/ m/s | 5.424942396 | | | | | |
| 3 | | $\omega_o$ / rads$^{-1}$ | 13.56235599 | | | | | |
| 4 | | Δt/s | 0.01 | | | | | |
| 5 | | Radius/m | 0.4 | | | | | |
| 6 | | | | | | | | |
| 7 | | | | | | | | |
| 8 | θi/rads | $\omega_i$ | $\dot{\omega}$ | ωf | Δθ/radians | T/s | θf/radians | θ/degrees |
| 9 | 0 | 13.56235599 | 0 | 13.56235599 | 0.13562356 | 0.01 | 0.13562356 | 7.770886768 |
| 10 | 0.13562356 | 13.56235599 | -8.289950993 | 13.47945648 | 0.135209062 | 0.02 | 0.270832622 | 15.51802388 |
| 11 | 0.270832622 | 13.47945648 | -2.62450659 | 13.45321141 | 0.134663339 | 0.03 | 0.405495962 | 23.23389244 |

**Fig 4:** The iteration constructed to predict the relationship between the vertical release height and the ride time. Microsoft Excel is used, and the input parameters are included. The first three steps are shown.

The approach velocity and radius are entered in cells C2 an C5. The angular velocity at the point of entry is entered into cell C3. A step size of 0.001s is chosen.

The first step begins with an angular displacement of $\theta=0^{\circ}$. In cell B9, the initial angular velocity is entered. In cell C9, the angular acceleration is determined according to Equation [7].

It is assumed that over the period of 0.001s, the angular acceleration remains constant. The angular velocity after a time interval of 0.001s is determined as the

product of the acceleration and the time interval (D9). The change in angular displacement during the step is then determined as the product of the average angular velocity and the time period.

$$\Delta\theta = (\frac{\omega_i+\omega_f}{2})\Delta t \quad [8]$$

The second step begins with an angular velocity equal to the angular velocity at the end of the previous step and a new angular acceleration is determined. This acceleration is used to find the angular velocity at the end of the second step and the process continues. As each steps proceeds, the cumulative angular displacement is found (Column H) and the gravitational potential and kinetic energies of the car are determined. By this means, the iteration can be used to plot the angular variation of the PE, KE and total energy. Figure 5, shows the data produced for a car of mass 100g entering a loop of radius 40cm with a linear speed of 6m/s.

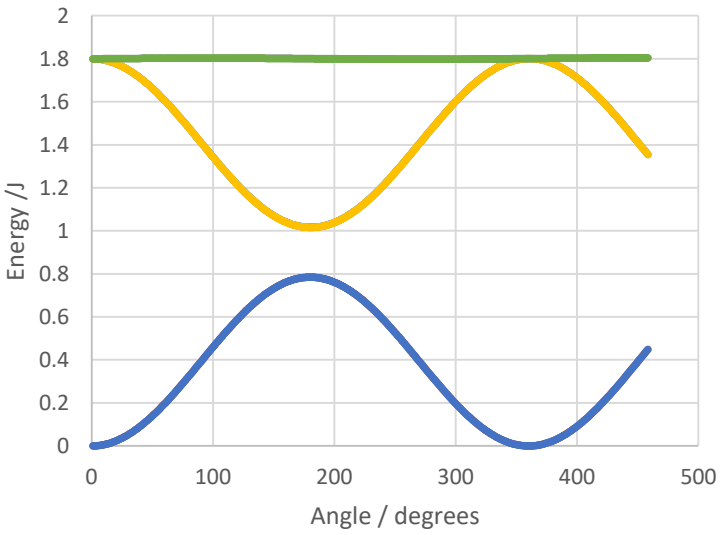


**Fig 5:** The iteration results for the angular dependency of the potential and kinetic energy in the absence of friction. Note that the total energy is constant.

### 1.2.3 Modification to account for frictional losses.

It is necessary to account for the role that frictional forces play in the angular acceleration and the torque experienced around the loop.

In the case of zero friction or a negligibly small coefficient of dynamic friction, the ratio $\frac{GPE}{KE}$ at any given point on the loop is independent of the approach velocity. The introduction of frictional force means that this is no longer true. Friction introduces an additional component to the torque. Unlike the torque due to gravity which alternates between opposing the angular motion (for angles 0 to π radians) and increasing the angular momentum (for angles π to 2π radians), the torque due to friction causes angular deceleration across the entire domain. The torque due to gravity is only a function of the angular displacement at a given point. Friction introduces a component of the torque which is dependent on both the angular displacement and the velocity. The frictional force is directly dependent on the normal reaction force and the reaction force is a function of the velocity. It seems likely that the fraction of the approach kinetic energy that is dissipated as heat will also be dependent on the approach velocity. Consider the case of a high approach velocity, the normal reaction force for a given angular displacement will increase due to the constraints of circular motion. This is expected to lead to greater net heat dissipation over a complete revolution, however this does not necessarily mean that the percentage heat loss relative to the approach KE is increased since a lower approach velocity will by the same argument produce a lower heat loss.

### 1.2.4 The effect of friction on the torque and angular acceleration

In order to develop an iteration that accounts for frictional heat losses, it is necessary to understand the relationship between the torque, the angular displacement and the angular velocity at a given position (figure 6).

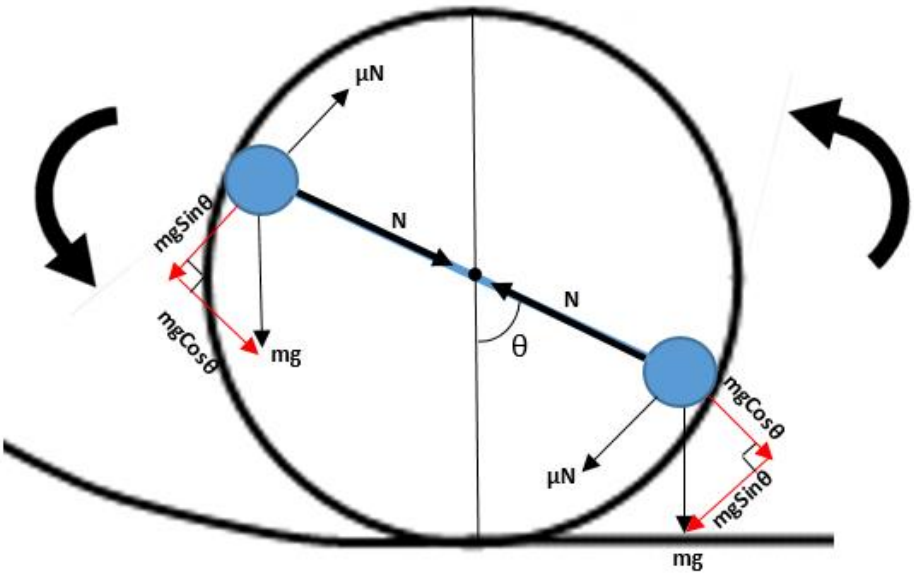


**Fig 6:** A diagram showing the car at key positions. The forces of gravity and friction are included.

Consider the car at point B. The torque due to gravity is given by:

$$\tau = -mg \sin\theta \quad [9]$$

The negative sign ensures that the torque opposes the angular momentum in quadrants 1 and 2, and works to increase angular momentum in quadrants 2 and 3. In the presence of friction, a new component of the torque is introduced:

$$F = \mu N \ [10]$$

Where μ is the coefficient of dynamic friction. This component is negative at all points on the circular path. Circular motion requires that:

$$\frac{mv^2}{r} = N - mg \cos\theta \ [11]$$

Thus, the magnitude of the normal reaction force is given by:

$$|N| = \left|\frac{mv^2}{r} + mg\cos\theta\right| \text{ [12]}$$

From equations [10] and [12] it follows that:

$$F = \mu\left[\frac{mv^2}{r} + mg\cos\theta\right] \text{ [13]}$$

The net force is given by:

$$F_{net} = -mg\sin\theta - \mu\left[\frac{mv^2}{r} + mg\cos\theta\right] \text{ [14]}$$

The force in equation [14] acts at 90° to the radius. Therefore, the net torque is given by:

$$\tau = -rmg\sin\theta - \mu mv^2 - \mu mg\cos\theta\, r \text{ [15]}$$

Interpretation of the result is made easier when expressed alternatively:

$$\tau = -rmg[\sin\theta + \mu\cos\theta] - \mu mv^2 \text{ [16]}$$

In the case of zero friction (μ = 0), the equation reverts to that developed due to gravitational effects alone.

Equation [16] can be expressed in terms of angular velocity:

$$\tau = -rmg[\sin\theta + \mu\cos\theta] - \mu m\omega^2 r^2 \text{ [17]}$$

It is now a simple task to modify the iteration, to account energy losses due to friction. This modification requires only the introduction of a new input parameter in the form of the coefficient of dynamic friction and the substitution of the friction free torque expression with that described by equation [17].

## 2.0 Practical methodology

The iteration allows for the theoretical relationship between the percentage energy loss and input velocity to be determined. These results are tested against practical measurements. A 0.4m radius roller coaster is constructed out of wood lined with flexible electrical conduit. The conduit is chosen so that it has a width equal to the wheel base of a model hot wheel car. The apparatus is shown in figure 7 below. Varying input velocities are achieved through altering the vertical release height. The motion is filmed at 240fps and analyzed using video analysis software (Tracker) to determine the initial and exit KE. Experimental results are compared to the iterated predictions.

**Fig 7:** Figure showing the apparatus.

## 2.1 Uncertainties in Raw and Processed Data

The principle source of uncertainty will be in the determination of kinetic energies. The mass of the car was measured as 33.62g ±0.01g. This error is negligible. The input and exit velocities were determined through video analysis. The software tracks at one frame intervals. The video file was recorded at a frame rate of 240fps. The software provides a velocity value for each tracking event. These velocities are averaged and the average deviation of the values from their mean is determined. The input velocities ranged from 5.2m/s to 6.1m/s, with average deviations ranging from 0.1m/s and 0.4m/s respectively. The output velocities ranged from 4.4m/s to 3.7m/s, with average deviations ranging from 0.0m/s to 0.3m/s respectively. An important input parameter for the correct functioning of the iteration is the coefficient of dynamic friction. This was obtained through measurements of the ride time. The ride time was determined through video tracking. There was an uncertainty of approximately 2 frames in establishing the moment of entry and of exit corresponding to a net absolute error of ±0.04s. This translated into a coefficient value of 0.09 with an error of ±0.01 (11%). This has an effect on the accuracy of the theoretical values.

## 2.2 Experimental Results

| $V_{in}$ (m/s) | $\Delta V_{in}$ (m/s) | $V_{out}$ (m/s) | $\Delta V_{out}$ (m/s) | $R_{T \pm 0.02s}$ | $KE_{in}$ (J) | $\Delta KE_{in}$ (J) | $KE_{out}$ (J) | $\Delta KE_{out}$ (J) | $\Delta Q$ (J) | %Lost | $\Delta\Delta Q$ (J) | Δ%Lost |
|---|---|---|---|---|---|---|---|---|---|---|---|---|
| 6.1 | 0.2 | 4.4 | 0.2 | 0.67 | 0.63 | 0.04 | 0.33 | 0.03 | 0.30 | 48 | 0.07 | 14 |
| 6.1 | 0.4 | 4.3 | 0.2 | 0.65 | 0.63 | 0.08 | 0.31 | 0.03 | 0.3 | 50 | 0.1 | 24 |
| 6.1 | 0.2 | 4.1 | 0.2 | 0.77 | 0.63 | 0.04 | 0.28 | 0.03 | 0.34 | 55 | 0.07 | 15 |
| 5.8 | 0.3 | 4.2 | 0.3 | 0.71 | 0.57 | 0.06 | 0.30 | 0.04 | 0.3 | 48 | 0.1 | 23 |
| 5.8 | 0.3 | 4.1 | 0.3 | 0.66 | 0.56 | 0.06 | 0.28 | 0.04 | 0.3 | 49 | 0.1 | 23 |
| 5.5 | 0.3 | 4.0 | 0.1 | 0.70 | 0.51 | 0.06 | 0.27 | 0.01 | 0.24 | 47 | 0.07 | 19 |
| 5.6 | 0.1 | 3.7 | 0.1 | 0.75 | 0.53 | 0.02 | 0.23 | 0.01 | 0.30 | 56 | 0.03 | 8 |
| 5.5 | 0.1 | 4.0 | 0.1 | 0.70 | 0.51 | 0.02 | 0.27 | 0.01 | 0.24 | 47 | 0.03 | 8 |
| 5.5 | 0.3 | 3.9 | 0.1 | 0.77 | 0.51 | 0.06 | 0.26 | 0.01 | 0.25 | 50 | 0.07 | 19 |
| 5.6 | 0.1 | 4.1 | 0.2 | 0.67 | 0.53 | 0.02 | 0.28 | 0.03 | 0.24 | 46 | 0.05 | 10 |
| 5.5 | 0.5 | 3.8 | 0.3 | 0.71 | 0.51 | 0.09 | 0.24 | 0.04 | 0.3 | 52 | 0.1 | 35 |
| 5.5 | 0.2 | 3.8 | 0.2 | 0.73 | 0.51 | 0.04 | 0.24 | 0.03 | 0.27 | 52 | 0.06 | 16 |
| 5.7 | 0.3 | 4.4 | 0.0 | 0.67 | 0.55 | 0.06 | 0.33 | 0.00 | 0.22 | 40 | 0.06 | 15 |
| 5.4 | 0.2 | 4.0 | 0.3 | 0.68 | 0.49 | 0.04 | 0.27 | 0.04 | 0.22 | 45 | 0.08 | 19 |
| 5.5 | 0.1 | 4.0 | 0.2 | 0.71 | 0.51 | 0.02 | 0.27 | 0.03 | 0.24 | 47 | 0.05 | 11 |
| 5.3 | 0.4 | 3.8 | 0.1 | 0.78 | 0.47 | 0.07 | 0.24 | 0.01 | 0.23 | 49 | 0.08 | 25 |
| 5.3 | 0.4 | 3.8 | 0.2 | 0.77 | 0.47 | 0.07 | 0.24 | 0.03 | 0.2 | 49 | 0.1 | 28 |
| 5.3 | 0.2 | 3.7 | 0.0 | 0.80 | 0.47 | 0.04 | 0.23 | 0.00 | 0.24 | 51 | 0.04 | 11 |
| 5.4 | 0.4 | 4.0 | 0.2 | 0.71 | 0.49 | 0.07 | 0.27 | 0.03 | 0.2 | 45 | 0.1 | 27 |
| 5.3 | 0.3 | 3.9 | 0.2 | 0.75 | 0.48 | 0.05 | 0.26 | 0.03 | 0.22 | 46 | 0.08 | 22 |
| 5.4 | 0.1 | 3.7 | 0.1 | 0.80 | 0.49 | 0.02 | 0.23 | 0.01 | 0.26 | 53 | 0.03 | 8 |
| 5.2 | 0.2 | 3.7 | 0.2 | 0.82 | 0.45 | 0.03 | 0.23 | 0.02 | 0.22 | 49 | 0.06 | 17 |
| 5.5 | 0.2 | 3.9 | 0.0 | 0.79 | 0.51 | 0.04 | 0.26 | 0.00 | 0.25 | 50 | 0.04 | 11 |
| 5.4 | 0.1 | 3.8 | 0.1 | 0.76 | 0.49 | 0.02 | 0.24 | 0.01 | 0.25 | 50 | 0.03 | 8 |
| 5.2 | 0.3 | 3.9 | 0.1 | 0.80 | 0.45 | 0.05 | 0.26 | 0.01 | 0.20 | 44 | 0.07 | 19 |

**Fig 8:** Raw data for, the input and output velocities. The table includes the derived data for the net energy loss within a complete loop and the corresponding percentage energy loss.

| $V_{in}$ (m/s) | $\Delta V_{in}$ (m/s) | $V_{out}$ (m/s) | $\Delta V_{out}$ (m/s) | $R_T$ ±0.02s | $KE_{in}$ (J) | $\Delta KE_{in}$ (J) | $KE_{out}$ (J) | $\Delta KE_{out}$ (J) | $\Delta Q$ (J) | %Lost | $\Delta\Delta Q$ (J) | Δ%Lost |
|---|---|---|---|---|---|---|---|---|---|---|---|---|
| 6.1 | 0.2 | 4.4 | 0.2 | 0.67 | 0.63 | 0.04 | 0.31 | 0.03 | 0.31 | 50 | 0.07 | 14 |
| 5.8 | 0.4 | 4.3 | 0.2 | 0.65 | 0.57 | 0.08 | 0.29 | 0.03 | 0.3 | 48 | 0.1 | 25 |
| 5.7 | 0.2 | 4.1 | 0.2 | 0.77 | 0.55 | 0.04 | 0.28 | 0.03 | 0.26 | 48 | 0.07 | 15 |
| 6.1 | 0.3 | 4.2 | 0.3 | 0.71 | 0.63 | 0.06 | 0.31 | 0.04 | 0.3 | 50 | 0.1 | 22 |
| 6.1 | 0.3 | 4.1 | 0.3 | 0.66 | 0.63 | 0.06 | 0.31 | 0.05 | 0.3 | 50 | 0.1 | 22 |
| 5.5 | 0.3 | 4.0 | 0.1 | 0.70 | 0.51 | 0.06 | 0.27 | 0.01 | 0.24 | 47 | 0.07 | 19 |
| 5.5 | 0.1 | 3.7 | 0.1 | 0.75 | 0.51 | 0.02 | 0.27 | 0.01 | 0.24 | 47 | 0.03 | 8 |
| 5.7 | 0.1 | 4.0 | 0.1 | 0.70 | 0.55 | 0.02 | 0.28 | 0.01 | 0.26 | 48 | 0.03 | 8 |
| 5.4 | 0.3 | 3.9 | 0.1 | 0.77 | 0.49 | 0.05 | 0.27 | 0.01 | 0.23 | 46 | 0.07 | 19 |
| 5.5 | 0.1 | 4.1 | 0.2 | 0.67 | 0.51 | 0.02 | 0.27 | 0.03 | 0.24 | 47 | 0.05 | 11 |
| 5.5 | 0.5 | 3.8 | 0.3 | 0.71 | 0.51 | 0.09 | 0.27 | 0.04 | 0.2 | 47 | 0.1 | 35 |
| 5.6 | 0.2 | 3.8 | 0.2 | 0.73 | 0.53 | 0.04 | 0.28 | 0.03 | 0.25 | 47 | 0.07 | 16 |
| 5.5 | 0.3 | 4.4 | 0.0 | 0.67 | 0.51 | 0.06 | 0.27 | 0.00 | 0.24 | 47 | 0.06 | 16 |
| 5.5 | 0.2 | 4.0 | 0.3 | 0.68 | 0.51 | 0.04 | 0.27 | 0.04 | 0.24 | 47 | 0.08 | 19 |
| 5.6 | 0.1 | 4.0 | 0.2 | 0.71 | 0.53 | 0.02 | 0.28 | 0.03 | 0.25 | 47 | 0.05 | 11 |
| 5.3 | 0.4 | 3.8 | 0.1 | 0.78 | 0.47 | 0.07 | 0.26 | 0.01 | 0.21 | 45 | 0.08 | 25 |
| 5.3 | 0.4 | 3.8 | 0.2 | 0.77 | 0.47 | 0.07 | 0.26 | 0.03 | 0.2 | 45 | 0.1 | 28 |
| 5.3 | 0.2 | 3.7 | 0.0 | 0.80 | 0.47 | 0.04 | 0.26 | 0.00 | 0.21 | 45 | 0.04 | 11 |
| 5.4 | 0.4 | 4.0 | 0.2 | 0.71 | 0.49 | 0.07 | 0.27 | 0.03 | 0.2 | 46 | 0.1 | 27 |
| 5.3 | 0.3 | 3.9 | 0.2 | 0.75 | 0.47 | 0.05 | 0.26 | 0.03 | 0.21 | 45 | 0.08 | 22 |
| 5.4 | 0.1 | 3.7 | 0.1 | 0.80 | 0.49 | 0.02 | 0.27 | 0.01 | 0.23 | 46 | 0.03 | 8 |
| 5.2 | 0.2 | 3.7 | 0.2 | 0.82 | 0.45 | 0.03 | 0.25 | 0.03 | 0.20 | 44 | 0.06 | 17 |
| 5.5 | 0.2 | 3.9 | 0.0 | 0.79 | 0.51 | 0.04 | 0.27 | 0.00 | 0.24 | 47 | 0.04 | 11 |
| 5.4 | 0.1 | 3.8 | 0.1 | 0.76 | 0.49 | 0.02 | 0.27 | 0.01 | 0.23 | 46 | 0.03 | 8 |
| 5.2 | 0.3 | 3.9 | 0.1 | 0.80 | 0.4545 | 0.05 | 0.25 | 0.01 | 0.20 | 44 | 0.07 | 20 |

**Fig 9:** The values for the net and percentage energy loss determined through the iteration. The coefficient of friction is found using the ride time for each event.

| $V_{input}$ (m/s) | Ride Time / s ±0.02s | μ |
|---|---|---|
| 6.1 | 0.67 | 0.11 |
| 5.8 | 0.71 | 0.1 |
| 5.7 | 0.66 | 0.08 |
| 6.1 | 0.65 | 0.11 |
| 6.1 | 0.77 | 0.15 |
| 5.5 | 0.71 | 0.08 |
| 5.5 | 0.73 | 0.08 |
| 5.7 | 0.67 | 0.08 |
| 5.4 | 0.68 | 0.07 |
| 5.5 | 0.71 | 0.08 |
| 5.5 | 0.7 | 0.07 |
| 5.6 | 0.75 | 0.1 |
| 5.5 | 0.7 | 0.07 |
| 5.5 | 0.77 | 0.1 |
| 5.6 | 0.67 | 0.07 |
| 5.3 | 0.78 | 0.09 |
| 5.3 | 0.77 | 0.09 |
| 5.3 | 0.8 | 0.09 |
| 5.4 | 0.71 | 0.07 |
| 5.33 | 0.75 | 0.08 |
| 5.4 | 0.8 | 0.1 |
| 5.2 | 0.82 | 0.09 |
| 5.5 | 0.79 | 0.1 |
| 5.4 | 0.76 | 0.09 |
| 5.2 | 0.8 | 0.09 |

**Fig 10:** The values for the coefficient of friction for varying input velocities determined through the iteration, from which the average value of the coefficient of friction and average deviation from the mean are determined.

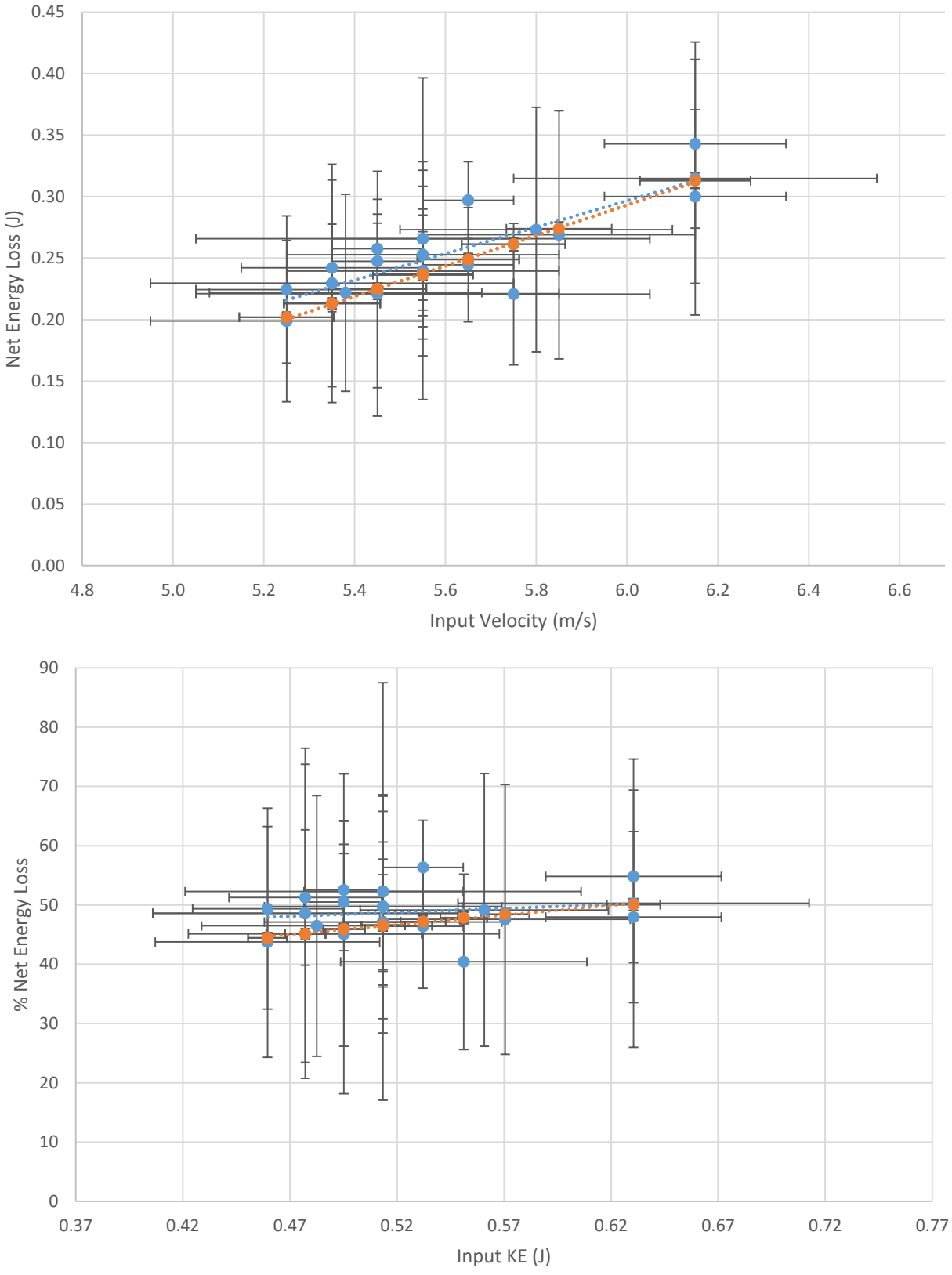


**Fig 11 & 12:** Graphs of net energy loss (top) and percentage energy loss (bottom) versus input velocity and KE respectively. The theoretical results are in red. Note that that horizontal axes are not origin zeroed.

## 3.0 Discussion

Before conclusions can be made regarding the relationship between the net and percentage energy loss and input velocity, it is necessary to consider the effect of experimental uncertainties in the processed data. The experimental findings are compared with theoretical values determined through numerical analysis. These values are subject to error due to uncertainties in the parameters.

Figures 11 and 12 show significant experimental uncertainties associated with the input kinetic energy and the percentage heat loss. Such uncertainties are to be expected since the kinetic energy is a function of mass and velocity. The uncertainty associated with the mass of the car is considered negligible. The uncertainty in the velocity measurements are largely independent of the velocity itself. These uncertainties are observed to range between ±0.1m/s and ±0.4m/s. The greatest fractional uncertainty occurs for the input velocity of 5.3m/s ±0.4m/s. This corresponds to an error of approximately 8%. The least fractional uncertainty is observed for the input velocity of 6.1m/s ±0.2m/s (±3%). These values lead to maximum and minimum uncertainties in the input kinetic energies of 16% and 6% respectively. Since the output velocity values are reduced due to energy losses, the fractional error on the exit KE values are greater than those of the input KE. The net energy loss is determined through subtraction, and the absolute uncertainties are added. The percentage energy loss is determined as the ratio of the net energy loss to the input KE. The fractional errors of both quantities are summed. This results in the uncertainties ranging from 8% to 35%.

Data determined through numerical analysis is subject to the precision of the input data. The iteration requires knowledge of the coefficient of dynamic friction and the approach velocity. The dynamic friction value was determined as 0.09 ±0.01 (11%) through ride time analysis. To see the effect of this on the iteration output, consider an

approach velocity of 5.3m/s. For an input coefficient of friction of 0.09, the iteration produces a final KE of 0.259J. For input values of 0.10 and 0.08, the KE values are 0.243J and 0.277J respectively. This implies an uncertainty of approximately 8%. The theoretical values for the net energy loss within a complete loop are also subject to the uncertainty in the velocity input data. Figure 13 shows the total energy loss within the loop for an entrance velocity of 5.3m/s ±0.4m/s. The red, orange, and blue lines show the energy loss versus angular displacement for the velocity of 5.7m/s, 5.3m/s and 4.9m/s respectively. It is interesting to note that the uncertainty in the value of the entrance velocity produces greater uncertainty in the iterated energy loss values for smaller angles.

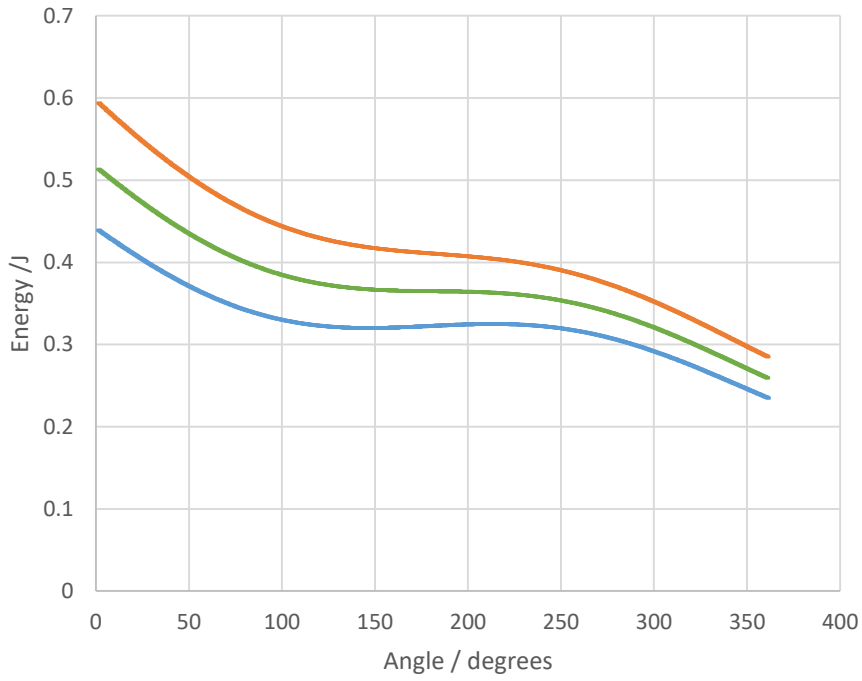


**Fig 13:** A graph illustrating the effect of input velocity uncertainty on the iterated values of energy loss.

The uncertainties associated with the input velocities over an entire loop produce error in the theoretical data in the order of 2% and these uncertainties are shown in figures 11 and 12.

The net energy loss as a function of the input velocity was studied. Numerical analysis was used to produce a set of theoretical data for a velocity domain of $5.2\text{m/s} < V < 6.2\text{m/s}$. The results are shown as the red data points in figure 11. A linear regression is applied to the data. Linearity is strongly supported by an $R^2$ value of 0.9992. The regression analysis suggested a negative intercept on the vertical axis of -0.44J. A negative kinetic energy is clearly impossible. However, it must be remembered that for all coaster loops there exists a threshold velocity below which the car will fail to make a complete revolution and as such, the presence of a negative intercept need not be problematic. The linear relationship suggested by numerical analysis is far from obvious and has interesting real life consequences in the design of multiple loop coasters.

The practical data is shown in blue. There is a strong agreement between theoretical and practical data over the velocity domain investigated.

In designing a multiple loop coaster, the ratio of the energy loss to the approach velocity is a key consideration. Figure 12 shows the iterated and practical data points for the percentage loss against the approach kinetic energy. The iteration results support a linear relationship with an $R^2$ value of 0.9913. For the least value of input KE (0.45J), a net energy loss of 44% is observed. For the greatest input KE (0.63J), the net energy loss rises linearly to a value of 50%. This implies that an increase in the approach KE by 40% leads to an increase in percentage energy loss of just 14%. Such a finding is beneficial in the design of high speed roller coasters.

The practical data (Fig. 12) supports the theoretical findings. A small degree of scattering is evident. There is close agreement between the two data sets. The greatest deviation between the practical data and theoretical data is observed for the input KE of 0.53J. For this value, the iteration predicts an energy loss of 47%, and the practical data suggests an energy loss of 56%. There is a tendency for the practical data to over read the theoretical predictions, however the practical values lie within the error bars associated with experimental uncertainty.

## 4.0 Conclusion

This paper set out to investigate two aspects of the energy loss incurred during a complete loop of a circular roller coaster. The first relationship explored is that between the net energy loss in a complete loop and the entrance velocity. The numerical analysis suggests a linear relationship. The iterated results are strongly supported by the practical data over the domain of the velocities investigated. The second aspect investigated was that of the percentage energy loss as a function of the input kinetic energy. The numerical analysis predicted a counterintuitive linear relationship. The practical evidence for this is less convincing due to the accumulation of uncertainty in the processed values, however the data does fit within the iterated values allowing for experimental uncertainties. The iteration and practical data suggests that the percentage energy loss is more significant for lower input kinetic energies. For the least kinetic energy investigated, it was found that 50% energy dissipation occurred. The data suggests that increasing the input KE by 14% causes the dissipation to rise to 50%. This observation has important implications when considering the design of circular or bi-circular clothoid coasters, since it infers that higher speed rides are essentially more efficient.

This paper was restricted to the study of energy losses within a circular loop. Most roller coasters employ a bi-circular clothoid approximation. It is not difficult to modify the iteration to account for the bi-circular rides. It would be interesting to carry out these modifications to see whether the linear observations observed in this paper, can be extended to bi-circular rides.

## 5.0 References:

*The Approximation of a Clothoid Curve, Commonly Used in Many Modern Roller Coasters*. Online photograph, "Roller Coasters and Amusement Park Physics," *The Physics Classroom*, 10 Jan. 2020, https://www.physicsclassroom.com/Class/circles/U6L2b.cfm.

Coker, Robert. *Roller Coasters: A Thrill Seeker's Guide to the Ultimate Scream Machines*. New York, Metrobooks, 2002.

*Multiple Loops in the Dragon Khan ride (Spain).* Online photograph, "Dragon Khan," *Rosenburg Blog*, 10 Jan. 2020, http://rosenburggdkegan.blogspot.com/2010/05/dragon-khan.html.

Pescovitz, David. "Roller Coaster." Encyclopædia Britannica, Encyclopædia Britannica, Inc., 20 Dec. 2019, 6 Jan. 2020, www.britannica.com/topic/roller-coaster.